Available online at www.CivileJournal.org

Civil Engineering Journal

Vol. 6, No. 11, November, 2020

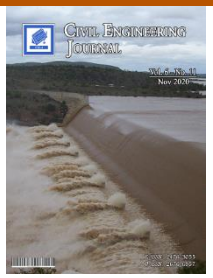

Flexural Behavior of Composite GFRP Pultruded I-Section Beams under Static and Impact Loading

Abbas A. Allawi [a], Safaa I. Ali [a*]

[a] *Department of Civil Engineering, College of Engineering, University of Baghdad, 10071, Baghdad, Iraq.*

Received 28 June 2020; Accepted 15 October 2020

Abstract

In this study, the effect of glass fiber reinforced polymer (GFRP) section and compressive strength of concrete in composite beams under static and low velocity impact loads was examined. Modeling was performed and the obtained results were compared with the test results and their compatibility was evaluated. Experimental tests of four composite beams were carried out, where two of them are control specimen with 20 MPa compressive strength of concrete deck slab and 50 MPa for other. Bending characteristics were affected by the strength of concrete under impact loading case, as it increased maximum impact force and damping time at a ratio of 59% and reduced the damping ratio by 47% compared to the reference hybrid beam. Under static loading, there was an increase in all the parameters, including the maximum load, ductility, and stiffness. Mid-span deflection was reduced by 25% under static and impact loads. A finite element analysis was performed by using the ABAQUS software. The midspan deflection value was greater than the experimental values by 6% and 3% for impact and static loads, respectively, and all other results showed a high rate of agreement with the obtained test results. The agreement between the numerical and experimental results indicates that the developed numerical model is capable of analyzing the impact and static behavior of such hybrid GFRP-concrete system.

Keywords: Glass Fiber Reinforced Plastics (GFRP); Concrete; Shear Connection; Hybrid Beams; Composite Beam; Pultruded FRP.

1. Introduction

Fiberglass Reinforced Polymers (FRP), also known as fiber-reinforced plastics or Advanced Composite Materials (ACMs), are composite materials made of a matrix of polymer resins reinforced with compact fibers typically glass, carbon, basalt or aramid. The polymer is usually an epoxy, vinyl or thermoplastic polyester or phenol-formaldehyde resin. The strength of the FRP fragment is mainly determined by the type of fiber and its orientation, amount and location within the fragment. The type of resin used determines corrosion resistance, flame retardant, and maximum operating temperature; it also significantly contributes to some strength characteristics including shock resistance and fatigue. There are many FRP products used in civil / structural engineering applications. Among those that have become increasingly common in the last two decades are structural Glass Fiber Reinforced Polymeric (GFRP) sections. Composite materials in the form of pultruded glass fiber reinforced polymer (GFRP) profiles have a great potential since they are economically affordable through the pultrusion process, which offers the best productivity/cost ratio of all the composites fabrication processes. However, when combined in a hybrid form with concrete, they have shown to offer excellent performance as floors, bridge decks, and beams when subject to static and impact loadings.

* Corresponding author: safaa.ib90@gmail.com

http://dx.doi.org/10.28991/cej-2020-03091608

The aim of this study therefore is to investigate experimentally and numerically the effect of concrete strength on the flexural behavior of a hybrid beam made of I section pultruded profile (GFRP) jointed with concrete by shear connectors.

2. Literature Review

The structural behavior of GFRP pultruded composite beams has been widely investigated through experimental and numerical studies Over the last two decades, many hybrid beams designs have been proposed and empirically analyzed, and the growing interest in this field of advanced composite materials has yielded promising results. The initial studies in this field were conducted by Bunsell and Harris, 1974 [1], who studied the behavior of CF and GF hybrid laminates embedded in an epoxy resin, either bonded or unbound. Bonded lamina better presented the behavior as elongation at failure than unbound specimens. Saiidi et al., 1994 [2] studied epoxy composite concrete beams for deck slab. They focused on the bending behavior of FRP I-section and the effects of concrete strength on the bond between I-section and concrete deck slab connected on epoxy layer. Joao R Correia et al., 2007; João Ramôa Correia et al., 2009; Fam and Rizkalla, 2002; Keller et al., 2007 [3–6] demonstrated that one way to improve the use of GFRP profiles is by connecting them with concrete elements in GFRP-concrete composite elements. Many hybrid concepts proposed by various authors aim to combine directionality, lightness, and high mechanical performance of FRP materials with the most relevant properties of conventional materials, especially concrete which is a less expensive and more massive material. Such a combination is typically visualized and tested in a structure supported simply by elements and leads to particularly useful solutions for the rehabilitation of old floors, resulting in increased synergy of rigidity and strength. Biddah, 2003 [7] and Fam and Skutezky 2006 [8] showed that the hybrid beams filled with concrete were less deformed and slippery compared to other samples, also they noted that concrete prevents local buckling of web and flanges.

Ferreira et al. 2004 [9] studied the properties of hybrid systems by using high-performance fiber reinforced concrete sheets, and characteristics and microstructures of hybrid sections were explored by Hai et al., 2010 [10]. A special hybrid profile of CFRP and GFRP layer was proposed by Mutsuyoshi et al., 2011 [11] in simple and complex compositions. Profile alone failed by bending due to crushing of web, while composite section showed a better performance in all sides. Gonilha et al., 2014 [12] found that the increased strength of concrete slab in GFRP-FSRSCc element of prototypical deck slab flexed the system and prevented failure. Nunes et al., 2016 [13] proposed experimental and numerical studies about the structural behaviors of GFRP and hybrid C-GFRP beams with unidirectional CF mats. The hybrid beam failed prematurely due to the delamination of CF mats located at compressed flange. In terms of stiffness and ultimate load, a good agreement with experimental results was found using numerical FE models, but the progressive delamination and failure behavior of the hybrid beams were not addressed.

M. Correia, 2012 [14] provided experimental, numerical, and analytical studies on the flexural behaviors of FRP, GF and CF fibers bound together and integrated into a polyester matrix. GFRP and five series of C-GFRP hybrid profiles, with different types and structures of CF reinforcements, underwent a four-point bending test to assess their structural response to failure, and experimental results confirmed the effectiveness of hybridization in increasing bending stiffness. Experimental tests were simulated using finite element models with the Hashin damage, a criterion to study material progressive failure and delamination. Numerical results showed good agreement with the experimental data in terms of the loading path and ultimate load.

Wayghan et al. 2019 [15] performed a parametric study to investigate the effects of pitch, concrete strength, column diameter, the quantity of longitudinal rebar and concrete cover. It has been shown that this rebar can contribute significantly in compressive strength of concrete columns if the column confinement is provided sufficiently. In order to achieve the required confinement to reach a sharp contribution of GFRP longitudinal rebar in concrete columns, the spiral of FRP rebar with small pitches around longitudinal rebar is taken into account. This leads to higher strains of concrete which can result in a higher contribution of FRP longitudinal rebar.

Zhang et al. 2019 [16] developed a guide line for the FE simulation of composite structures using the Hashin damage analysis available in ABAQUS. Both aerospace carbon/epoxy composites and civil engineering pultruded GFRP laminates were simulated and the numerical results obtained were consistent with the corresponding experimental data. The authors used material properties available in the literature and defined a sequence of steps and provided some recommendations for an efficient and accurate simulation.

Sun et al. 2019 [17] al investigated the behavior of GFRP-concrete beams made with GFRP tube profiles. The shear transfer mechanism consisted of conventional studs which had been used for steel-concrete composite beams, arranged in a cross-stitch pattern to prevent cracking between holes. There was no buckling of the hybrid specimens observed; however, the failure was sudden and occurred in the web of the profiles. The experimental behavior was linearly elastic up to failure and slip between the two materials was noted.

Design methods were also evaluated based on the Italian Manual and the American, and it was noted that the former was more accurate and conservative than the last. The current study shows that it is still necessary to conduct experimental research on beams and structural hybrid solutions in FRP-concrete hybrid beam at lower costs. In addition, a number of studies at this stage limited their analyses to full shear reaction, although slip events were previously observed during the test.

3. Experimental program

The main objective of this experimental study was to evaluate the advantages of introducing high-strength concrete in all hybrid beams subjected to bending. For this purpose, four concrete-GFRP hybrid beams were prepared and tested in three-point bending up to failure under static (CN, CH) and impact (CNI, CHI) loading conditions. These tests allowed assessing the influence of concrete strength in stiffness, ultimate loads, failure modes, and damping times of hybrid beams. Details and dimensions of the hybrid beam are shown in Figure 2.

Table 1. Experimental parametric details of experimental composite beams

Beam Designation	Strength of Concrete		Type of Loading	
	Normal	High	Static	Impact
CN	√		√	
CH		√	√	
CNI	√		√	√
CHI		√	√	√

4. Materials and Methods

The concrete mix was prepared to fabricate experimental specimens using cement Type I which tested according to (ASTM-C33 2016) [18], coarse aggregate of 12 mm maximum size and fine sand which tested according to (ASTM-C33 2016) [18]. Figure 1 shows the sieve analysis results for fine and coarse aggregate. To estimate the concrete compressive strength for each experimental specimen, three concrete cylinders with 150 × 300 mm dimensions were made and tested according to (ASTM C39-86 2002) [19]. All composite beams were reinforced in tension zone by deformed welded steel wire reinforcement (locally known as BRC) of 6 mm diameter spaced at 150 mm was used as flexural reinforcement (minimum ratio) for the produced concrete decks. Two wire specimens were cut from a (6×2) m dimensioned reinforcement, prepared and tested in tension as per the specification of ASTM 1064/1064M-14 with fy of 568 MPa which tested according to (ASTM A615/A615M-16) [20].

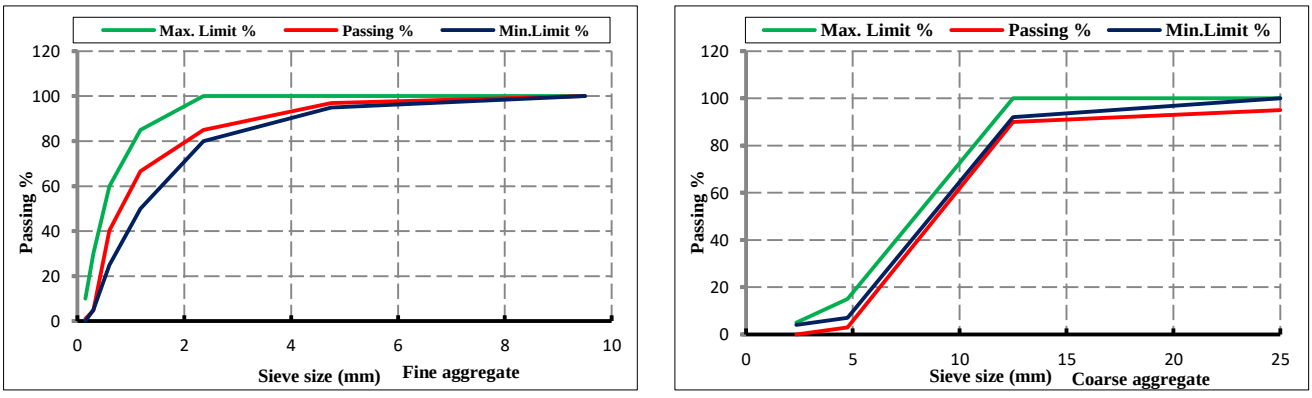

Figure 1. Sieve analysis results for fine and coarse aggregate

4.1. GFRP Pultruded I-Section

The I profile used in the experimental program consisted of a pulsed polyester matrix reinforced with E-glass fiber. Original profile couplings have been used for a wide range of mechanical features related to tension and complex, flexible and cutting characteristics [21, 22]. I-shaped GFRP section with 10-mm thickness was used for web and flanges (100-mm flange width and 150-mm total height as shown in Figures 2 and 3).

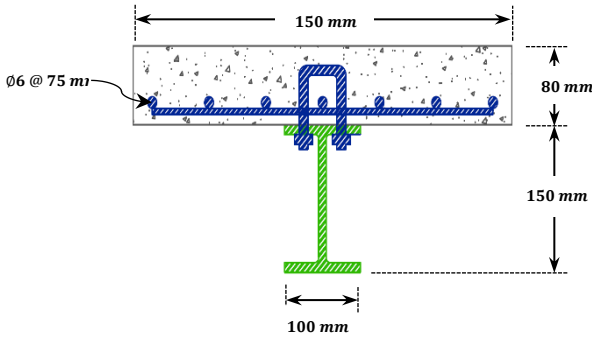

Figure 2. GFRP–concrete hybrid section geometry (dimensions in mm).

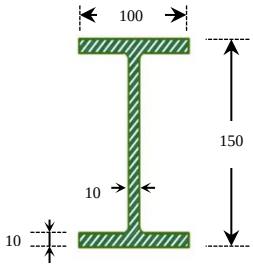

Figure 3. Cross section details (all dimensions in millimeter)

4.2. Shear Connectors

An inverted U-shaped hook was used to achieve a link between the GFRP and the concrete roof. The adhesion between GFRP and concrete was insignificant, and therefore, the entire shear connection was provided by mechanical contact. Punching shear test was carried out to analyze the behavior of the connection between GFRP and concrete and to use the findings in designing spacing between shear connectors. In punching shear connection tests, the flanges of a segment of the GFRP profile used in the hybrid beam were connected to two concrete prisms with hooks (Figures 4 and Figure 5). The profile was then loaded in compression until failure. The load was applied monotonously until the separation of the material occurred. The results given for the stiffness of the connections were estimated according to the definition provided by Johnson and May, 1975 [23]. Material separation suddenly occurred due to shear failure of the hooks under a maximum load of 159 kN (79.5 kN/mm per flange), see Figure 6. During the test, for high loads, deformation increased significantly. The high-pressure stress at the edge, in front of the hooks, indicated that failure was imminent. Punching shear connection tests proved the advantages of using high-grade concrete.

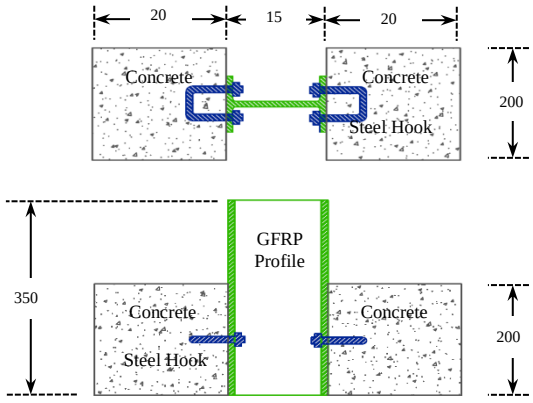

Figure 4. Geometry of the test specimen (mm): plan (top) and section (bottom)

Figure 5. Shear connection test setup

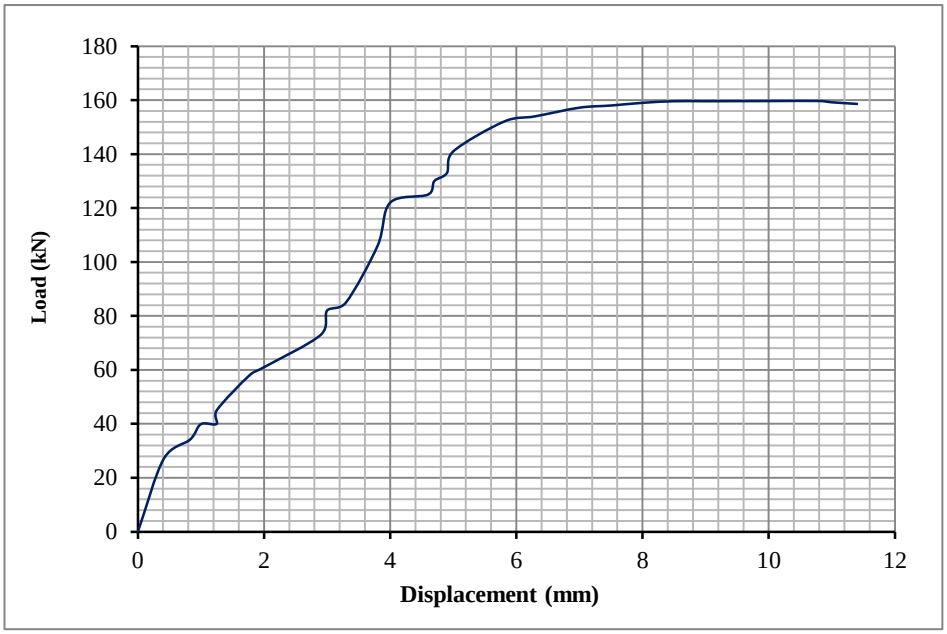

Figure 6. The load-displacement relationship

5. Fabrication and Experimental Setup for GFRP Concrete Hybrid Beams

5.1. Fabrication and Properties

Hybrid beams with a total length of 3000 mm underwent bending test under a single-point- load at the span of 2600 mm. The cross-section's dimensions for hybrid beams were selected for the two hybrid beams (in order to determine the compression deficit of concrete with a neutral axis inside the concrete slab) according to the preferential application of this type of structural element, especially for the restoration and reinforcement of concrete slabs. As a result, concrete slabs with a thickness of 80 mm and a width of 500 mm were accepted. Based on the results obtained during the shear connection test and the maximum compression load applied to the concrete slab, a spacing of 300 mm was adopted between the shear connection elements. Steel hooks, similar to those used in the shear connection tests, were previously placed in holes drilled in the upper flange and manually fixed as shown in Figure 7. Then, the slabs were cast against the beam top flange.

Figure 7. Preparation of the hybrid beam

5.2. Experimental Setup and Instrumentation

All supports were rotated freely. The load was applied using hydraulic jacks as presented in Figure 8. The load was measured with the load cells. Displacement transmitters (LVDT) and strain gauges were located at several intersections of the hybrid beam (Figure 9). The displacement transmitter δ_1 was used to measure the deflection in the middle of the S_1 portion of the two hybrid beams. Strain gauges ε_1 to ε_5 be connected to S_1 to evaluate deformations along the length of the section. To study the shear distribution between the concrete slabs and the GFRP profile's web, six elements (ε_6 to ε_{11}) were attached in section S_2 forming rosette in each element.

Figure 8. Flexural test setup—hybrid beam

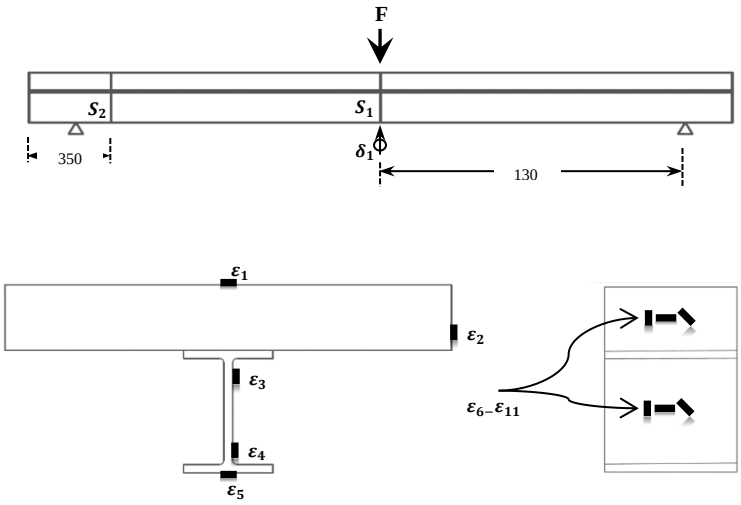

Figure 9. Hybrid beams instrumentation (mm): frontal view (top), section S1 (bottom left) and frontal view of section S2 (bottom right)

6. Results and Discussion

6.1. Experimental Results

The main purpose of the present research was to study the effect of two types of loads on (profiled GFRP I-Section and concrete deck slabs) the strength and performance of composite beams under monotonic static and impact loads.

6.1.1. First Part (Impact Test Results)

Two simply supported composite beams (CNI, CHI) were tested under impact loading (low-velocity impact). Strong steel frame and heavy to hold rigidly during impact loading by connected all structural elements to build the frame. Figure 10 shows sketch for steel frame that manufactured for impact tests to allow observing the specimens from the bottom surface to show developing of failure during testing. Steel mass of 25 kg are provided and dropped freely without any external force to the specimen that was placed accurately in the middle of the testing frame.

According to the results of the tests with accepted parameters, the observed and recorded points of the tests were as follows. The short-term duration of applied loads was the main difference between the impact and static tests. The sample was initially placed on the steel frame testing machine and then deflection sensors; force sensor and LVDT were set at certain points. In general, the applied force, deflection and tension behavior were not mathematically linear and there were many different points of view, such that the readings changed in value over time. Initially, the readings were of little value because they were used for a short time. At a certain time, depending on different variables such as

the compressive strength of concrete, the readings change in value and many of these readings will take place at times and then disappear. Test results showed that the peak impact force and mid-span deflection increased as the height of freely dropped mass because of increasing the stroked velocity. Cracks occurring on the concrete surface as a result of the impact test are local cracks in and around the drop zone. These cracks are not considered residual for static tests. The cracks for all the samples are the same in configuration but differ in intensity. As the compressive strength of concrete increases, cracking decreases.

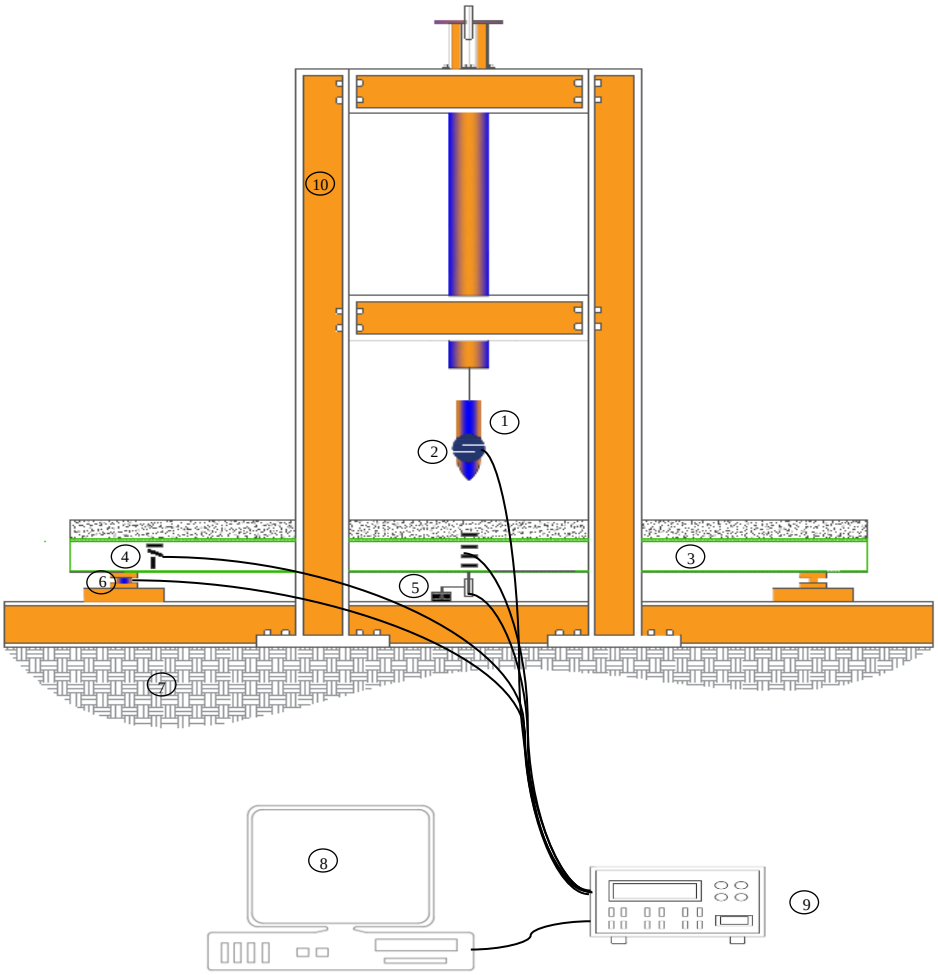

1- Impact mass.
2- Load cell.
3- Test Beam.
4- Strain Gauges.
5- LVDT.
6- Load cell under support.
7- Rigid floor.
8- Computer.
9- Data logger.
10- Frame

Figure 10. Impact test Machine

6.1.1.1. Maximum Impact Force and Maximum Deflection

Table 2 lists the results of the beams tested, maximum impact force, maximum deflection as a function of time, penetration to the upper face of the beam, and residual deformation. The bending time history and deformation have different values depending on the evolution of the compressive strength of the concrete. The modification (increase) of the concrete strength reduced the maximum deformation of the samples compared to the reference by 10% and the impact force increased due to the capacity of the concrete to absorb a larger amount of energy before failure.

Table 2. Specimen's test results for different drop heights

Height of drop (mm)	Name of specimen	Maximum Impact force (kN)	Maximum deflection (mm)	Penetration depth (mm)	Residual deflection (mm)
100	CNI	9.95	4	-	0.54
	CHI	11.2	3.62	-	0.43
500	CNI	23.0	9	0.2	3.9
	CHI	24.8	8.3	0.3	3.1
1000	CNI	34.13	12.3	1.1	6.43
	CHI	35.7	12.32	1.2	6
1500	CNI	39.4	15.4	2.2	10
	CHI	44.4	14.9	2.2	9.6
2000	CNI	50.1	19.68	4	13.3
	CHI	50.5	14	4.3	10.8

6.1.1.2. Load Under Support

Impact load is measured by stabilizing the load cell sensor under support. Increasing concrete strength of composite beams reduces absorption by 5% due to the increased stiffness of the composite beams caused by enhanced strength of concrete (Figure 11).

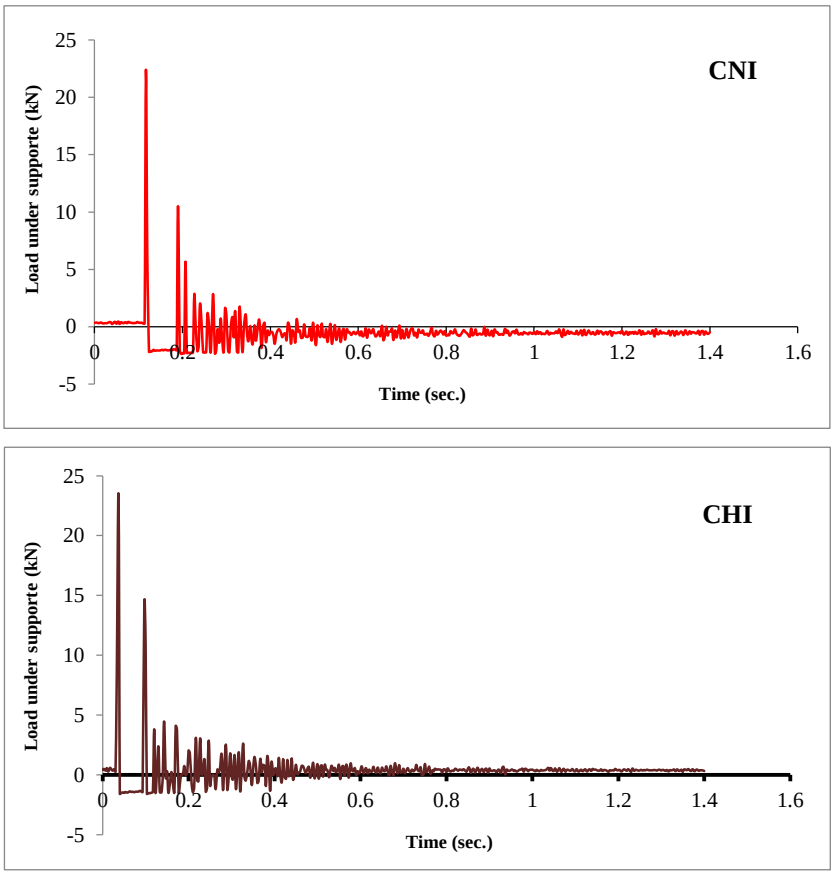

Figure 11. Relationship of load under support for hybrid beams

6.1.1.3. Damping Time

The time needed to reach 10% of the maximum deflection is called damping time, that is, the time required to reach 90% of the damping [24]. The damping time for the hybrid beam (CHI) is 1.95 s, which increases by a ratio of 59% compared with the reference hybrid beam (CNI) due to increase in the vibration period with enhancing the compressive strength of concrete. Shows the deflection - time relationship and damping time compared to the reference hybrid beam.

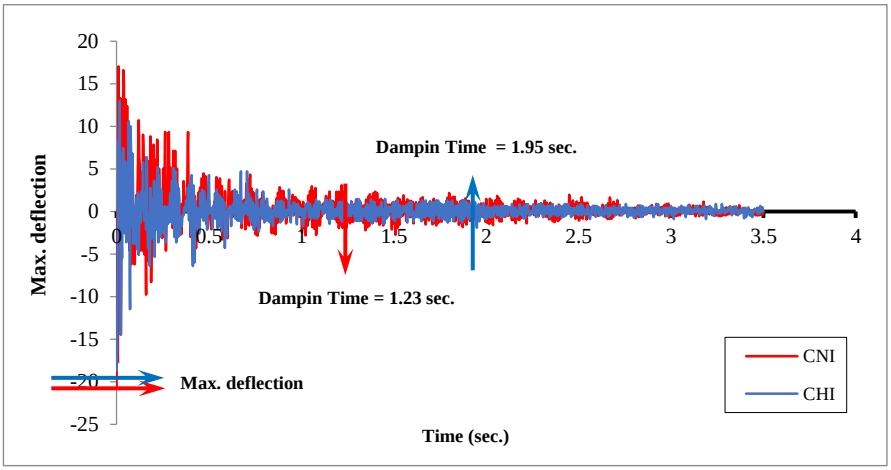

Figure 12. The deflection - time relationship and damping time for hybrid beam (CHI) compared to the reference hybrid beam (CNI)

6.1.1.4. Damping Ratio

The damping ratio is defined as the ratio of the viscous damping coefficient to the critical damping coefficient. It is designated by ζ (zeta), particularly important in the study by Alciatore, 2007 [25].

• **Experimental measure of damping ratio - logarithmic decrement**:

In this relationship, deflection has reduced from one peak to another until reset. A convenient way to measure the damping present in a system is to measure the rate of decay of free oscillations [26]. The higher is damping, the greater is the rate of decay (Figure 13), and the damping ratio was calculated by the following equations:

$$\delta = \frac{1}{n-m}\ln\left(\frac{\upsilon_m}{\upsilon_n}\right) \quad (1)$$

$$\zeta = \sqrt{\frac{\delta^2}{4\pi^2+\delta^2}} \quad (2)$$

Where n and m are deflection at peaks (υ_m, υ_n), respectively.

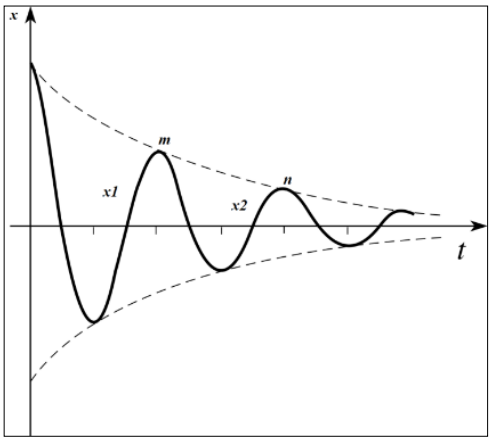

Figure 13. Rate of oscillation decay

Increase in the compressive strength of the concrete resulted in a reduction in the damping ratio by 47%, which signifies an inverse relationship between the damping time and the damping ratio.

6.1.2. Second Part (Static Test Results)

Four specimens were statically tested (CN, CH, CNI, CHI), each hybrid beam was loaded under incremental mid-span concentrated load at the top face of the beam up to failure. Two of the specimens were tested statically after the impact tests had been completed, and the other specimens were tested under static load only. LVDT were fixed at the mid-span bottom point of the beam to measure mid-span deflection.

The test results for loading capacity, deflection and strains in concrete and GFRP pultruded section are recorded and plotted.

6.1.2.1. Flexural Behaviour and Failure Modes

During the test, approximately linear behavior was observed in hybrid beam samples to failure. The connectors prevented separation in the GFRP section interface and concrete deck, but on the lower GFRP flange higher tension and lower compression stress of the upper flange were observed. This shows that the GFRP can be better utilized at high stress by taking advantage of the high compressive strength of concrete. The applied load and mid-span deflection were recorded for each tested hybrid beam and plotted as load mid-span deflection curves, generally indicating that all the samples increased with the applied load. Cracks in the concrete occurred, but there was some change in the slope of the linear relationship when the applied load reached approximately 70% of the final load for most tested beams. As a result, the linear response tended to take a nonlinear shape as the applied load increased. This indicates that the hybrid beam was about to collapse when the axis grew more rapidly with the application of the load. The load was applied monotonically, and as the compression, shear progressed along the length and depth of the region sets, the final failure of all the set suddenly occurred. This resulted in laminar shear of the web profile approximately 1 cm above the average depth with the beam splitting in two parts along the length of the beam. Laminar deficiency occurred after group delamination and transverse bending of the web (Figure 14).

At the beginning of the tests, large vertical flexural cracks appeared in the hybrid beam concretes due to the loss of strength of the material, as revealed by the jumps in the load displacement responses shown in Figure 15. As the loading progressed, the cracks proceeded towards the lower central part of the upper slab. The failure of the CH hybrid elements began with the crushing of the mid-span concrete top and was completed moments later when the bottom flange of the profile suddenly broke away from the GFRP sheet. The cause of the fragile collapse was determined as the increased shear stress at the junctions of the wings and ends of the pultruded elements. For the hybrid beams (i.e., CN and CHI), the failure began with a crushing of the concrete surface, followed by fragile shear delamination at one of its ends and at the junction between the upper flange and the web of the GFRP profile. The shear failure immediately dispersed to the middle portion of the beam, causing additional vertical movement of the steel hooks and local buckling of the compressed web (post-failure mechanism). In contrast, the CNI hybrid beam failure occurred suddenly at mid-span, without crushing the concrete, in the area directly under the applied load.

Figure 14. Failure of hybrid beam (cracking in concrete and inter-laminar shear failure)

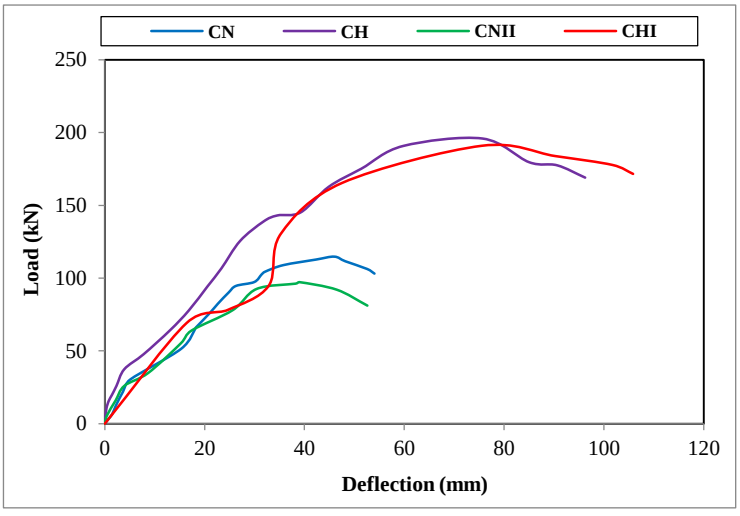

Figure 15. The load relationship with the mid span deflection

6.1.2.2. Composite Action and Interlayer Slip

Strain gauge performed at section S1 was used to determine the variation of longitudinal deformations in the applied load function. Figure 16 illustrates this change in the particular case of hybrid beams. Similar deformations between the upper slabs indicate that the entire width of the concrete slab is effective. This result is in line with the recommendations of the design code for simply supported reinforced composite beams [27]. The negative strain values recorded near the top flange of the GFRP profile indicates that the compressed element started to operate at higher load levels. Concrete strip curves for samples that failed mainly due to crushing of the slab showed the negative maximum values of 0.3%. The same information was used to plan axial deformations as a function of beam depth for different load levels. In this way, a better view of the composite action in the hybrid beam was obtained, while the slip tension at the interface between the concrete deck slab and the GFRP section was recorded in the hybrid beam plot. An example is shown in Figure 17 for the CN hybrid beam. An advanced sliding tension between the concrete slab and the profile results in the formation of two neutral axes at the intersection of the element. The first neutral axis of the T-shaped beam is placed inside the concrete slab, near the level of the steel frame, and the second neutral axis moves from the junction level to the center of the composite member due to the relatively low elastic modulus of GFRP. Slip tension values in the interface between materials were evaluated assuming that Bernoulli's hypothesis was applied separately to each element. Although the slip value estimates are only two measurements on each element of the hybrid beam, the results show that the interface between the two materials slips increases with load value. Non-linear behaviors (i.e., experimental friction, continuous/discrete contact, non-material laminates, etc.) are caused by a number of factors in the experiment.

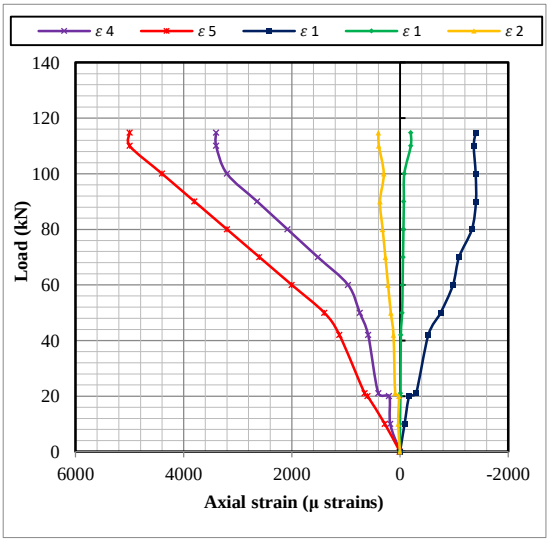

Figure 16. Hybrid beam CN, section S1: variation of axial strains in function of the applied load

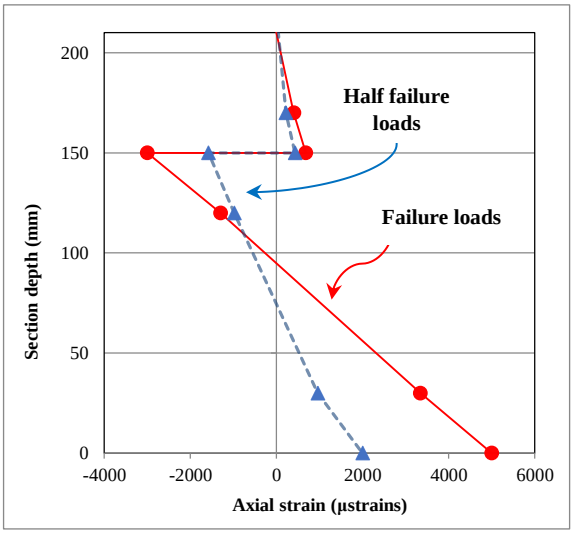

Figure 17. Hybrid beam CN, section S1: normal strain distribution at different load levels (kN)

6.1.2.3. Shear Strain Distribution

The results of the rosette strain gauges attached to the S_2 section profiles (in the middle, see Figure 18) were used to estimate the shear distribution between the GFRP profile and the concrete slab. In the GFRP profile, the results show that the profiles absorb more than 45% of the load and fail because of non-linear behavior of the concrete and secondary crushing. The value is approximately 70% of the total shear.

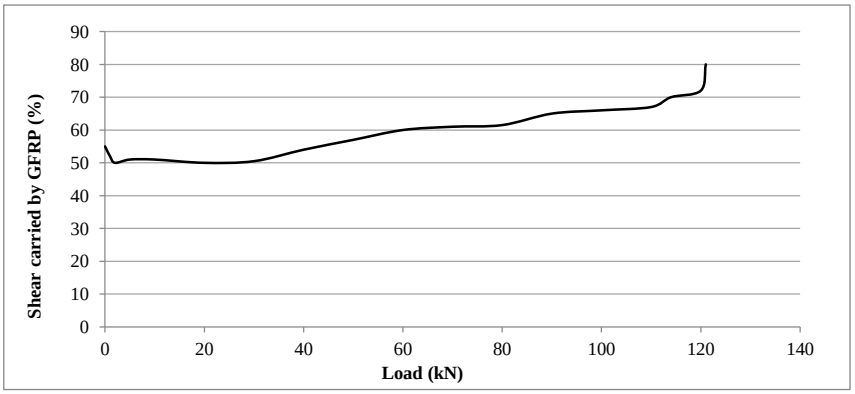

Figure 18. Shear carried by GFRP versus load for hybrid beam CN

6.2. Numerical Modeling

6.2.1. Finite Element Method

A numerical approach was adopted for finite elements: three-dimensional modeling composite beams (GFRP) were tested under impact and static loads. The ultimate analysis of elements with ABAQUS version 6.14 package consisted of real-time experimental simulation on beams to be examined. The composite beams, consisting of GFRP, deck slab and shear connectors, were modeled under 3D stress element for all the components, except for reinforcement steel which was modeled using standard 2D elements.

The concrete volume was represented by an eight-node solid brick element (C3D8R) with 2×2×2 integration points. The longitudinal and transverse steel rebars of these beams were modeled using an embedded truss reinforcement of 2-node linear 3D truss element (T3D2). Eight-node solid elements were also used to model steel plates under the applied load and the resisting reactions (Figure 19). It is worth mentioning that in this numerical analysis, the perfect bond was assumed between the surrounding concrete and the steel rebars (i.e., full compatibility). The damaged plasticity model (DPM) was used for the analysis. This model uses a combination of non-associated multi-hardening plasticity and scalar (isotropic) elasticity to describe the irreversible damage that happens during the fracturing process. The main two failure mechanisms adopted by this model are the tensile cracking and the compressive crushing of concrete. Numerical methods are the most effective engineering analysis techniques that can handle complex geometries. Among the many methods, finite element analysis (FEA) is one of the most versatile and comprehensive techniques currently available to engineers [28].

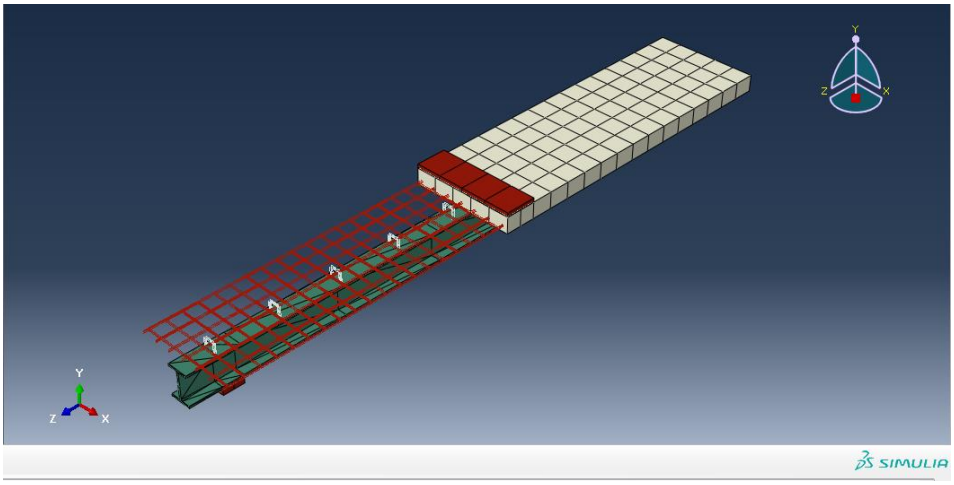

Figure 19. Model meshing for the composite beam

6.2.2. Material Models

Two material models of high-performance concrete and pultruded GFRP composites were used in this study. The concrete section of the hybrid beam was modeled by the use of concrete damaged plasticity model (CDPM) and, the pultruded profiles were modeled using the FRP composite material model (Hashin damage model). For the compressive behavior of concrete, two stress-strain relationship models were used to represent the ascending and descending zone respectively. Were used to describe the compressive hardening behavior (ascending zone).

6.2.2.1. Impact Loading

ABAQUS uses the load-time curves of the experimental study to check parameters such as deflection, strain and stresses as a function of time for analysis. A hollow solution was used to solve the equation set to identify the unknown variable (this method was included in the ABAQUS program). Multiple models ABAQUS adopts a finite element approach to simulate some of the tested beams in order to verify the complete operation of the hybrid beams subjected to static and impact loads. The maximum transient intermediate defect is an important indicator for assessing the damage levels caused by hybrid beams exposed to shocks. The results of the numerical models are related to the test results. Therefore, the supported load is more appropriate than the maximum effect and the specific result of maximum deflation. The predicted results were compared to the experimental ones. Taking the 2000 mm dropping height case (impact velocity = 6.26 m/s) as an example, as shown in Figure. 20, localized concrete crushing occurred at the impact area.

According to FEA results, CNI beam maximum mid-span deflection was 19.1 mm (as shown in Figure 21 compared to 20.65 mm of the experimental test. Load under support was 24.2 kN, while it was 22.4 kN in experimental results for the hybrid beam (CNI). Figure 21 shows a comparison of load under support, which indicates a good agreement between the experimental results and those of FEA.

Loading history and impact performance

The comparisons of the numerical and experimental results for one loading histories are shown in Figure 19. A reasonably good agreement is achieved between the experimental results and numerical ones. The typical loading histories for all impact energy levels can be divided into two stages, inertial resistance stage and dynamic bending resistance stage. Just after contact is initiated between the impactor and the top surface of the hybrid beam, the first stage is represented by a significant rapid increase in load to the maximum value, and dropping back to zero. In this stage, the impact force is represented by a rapid, short peak of inertial force due to the striking drop mass on the contact zone. The inertial force increases and then decreases quickly as the velocity of the hybrid beam increases. In the numerical prediction, the impactor was modeled as a rigid part instead of a steel impactor. This could explain why the predicted values in this stage are relatively higher than the experimental ones. The true impact resistance of the hybrid beam is represented by the second stage. In this stage, the hybrid beam starts to carry the impact load until failure occurs. Multiple failure mechanisms occur in this stage, including the debonding failure between the concrete and the profiles and the fracture of the concrete. The average difference between experimental results and numerical ones is only 7.4%. The numerical predictions are found to corroborate the experimental results in terms of failure modes and impact performance.

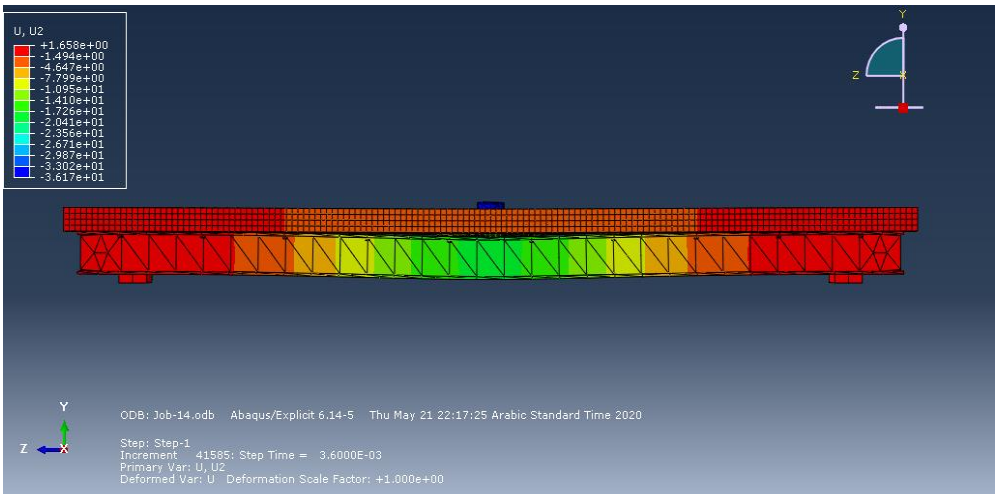

Figure 20. Analysis results of mid-span deflection of the hybrid beam under impact load

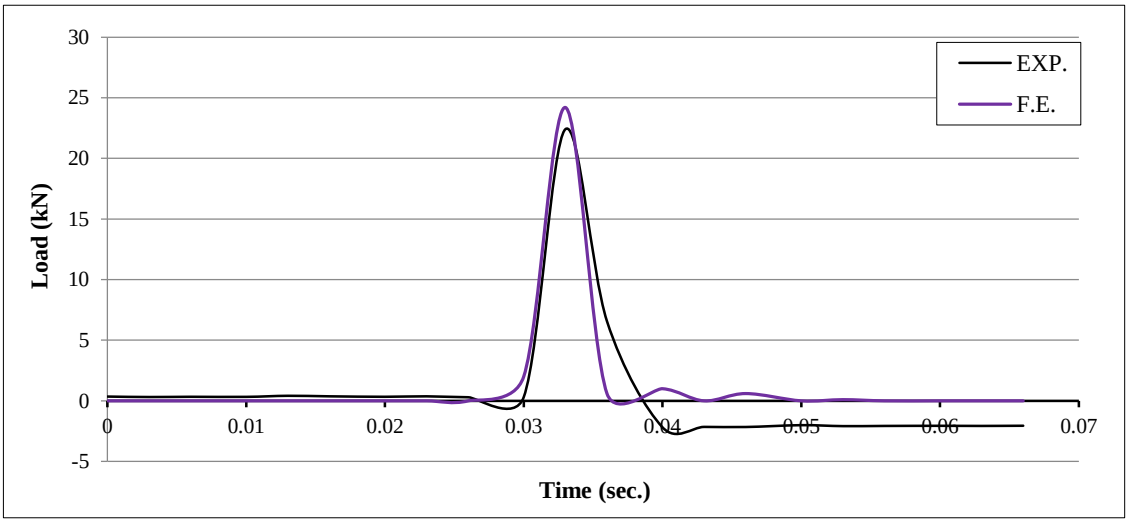

Figure 21. Experimental versus finite element load under support curves of the hybrid beam (CNI) (second stage)

6.2.3. Static Loading

Several comparisons are made with the experimental results. These include load-deflection relation and ultimate load capacity.

- Model subjected to static loading was simulated and the results were obtained.

- Model under impact loading was simulated and the results were obtained. The model was then (after the complete solution of impact analysis) subjected to static loading that was similar to that in experimental tests up to ultimate loading. The results from the ABAQUS model showed a close agreement with the experimental findings for load and deflection.

Under the same ultimate failure experimental load, the analysis for the hybrid beam (CN) yielded a deflection value of 42.6 mm compared to 46 mm in the experimental results. Figure 22 indicates a good agreement between the numerical and experimental results.

For the composite beam (CNI) subjected to impact load first, as seen in Figure 23, the load-displacement curves of the experimental analysis and FEA approximately coincided up to about 25% of the ultimate load, after which the FEA curve diverged slightly upwards and its path became parallel to the experimental curve. Although the difference was not significant, and as per the researcher's point of view, after applying the impact force, the cracking in concrete propagated and the concrete grew weak. For this reason, the GFRP beam became dominant in behavior. The GFRP material composition and manufacturing process cannot be 100% guaranteed in uniformity and distribution of glass fiber reinforcement within the matrix resin of multilayer. But, FEA simulation assumes ideal uniform material properties of the modeled part.

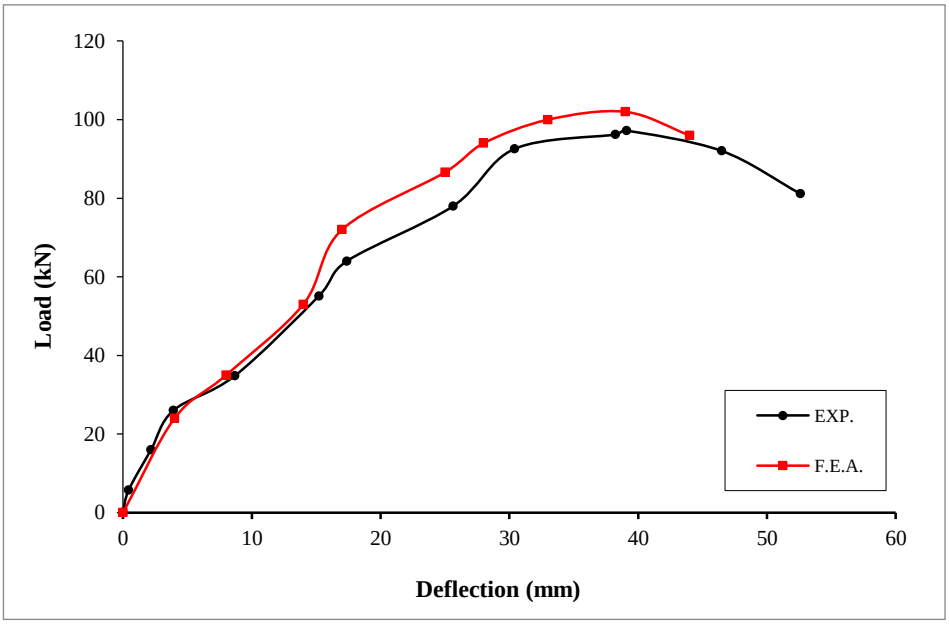

Figure 22. Experimental vs. FEA load-deflection curves of hybrid beam CN

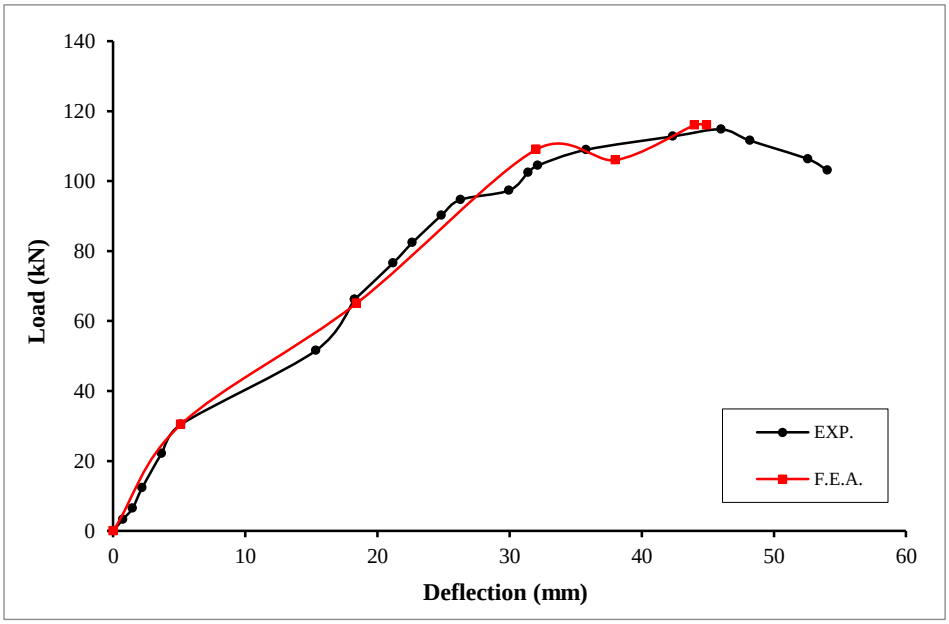

Figure 23. Experimental vs. FEA load-deflection curves of hybrid beam CNI

7. Conclusions

Based on the results of experimental work and numerical analysis of this research, the following main conclusions can be drawn:

- The addition of concrete deck provides an extra resistance to the compression flange of the GFRP section. This reduces the compressive strains (and stresses) on section top flange and pushes GFRP section bottom flange to exhibit its reserved tensile strength which definitely increases the total strength of hybrid beam;
- The type/configuration of support considerably affects the obtained failure mode and strength capacity of hybrid beam. As far as symmetry is assured, higher failure strength is obtained;
- The similarity in modes of failure of most hybrid beams by inter laminar shear failure reflects a weakness in the region of flange to web junction of GFRP section. This necessitates some measurements to be taken by manufacturers during the fabrication process to strengthen this region, whether it is related to fiber reinforcement or matrix resin content;
- The maximum measured normal strains in concrete deck did not reach the ultimate values of 0.003. Hence, there should be extra compressive strength in concrete which may be utilized by using shear connectors with closer spacing to a certain limit. This in turn, enhances (to some degree) the composite action of hybrid beam and raises its strength;
- The stiffeners of GFRP–concrete hybrid beams increased the strength of composite beams and damping time and reduced the damping ratio, the damping time for the hybrid beam (CHI) is 1.95 sec, which increases by a ratio of 59% compared with the reference hybrid beam (CNI) and reduction in the damping ratio by 47%, due to increase in the vibration period with enhancing the compressive strength of concrete;
- The modification (increase) of the concrete strength reduced the maximum deformation of the samples compared to the reference by 10%;
- The results show that the profiles absorb more than 45% of the load and fail because of non-linear behavior of the concrete and secondary crushing;
- Impact test result showed a decreased in deflection value for hybrid beam with (high strength concrete) by 40.5 % compared with hybrid beam with normal strength concrete.

8. Conflicts of Interest

The authors declare no conflict of interest.

9. References

[1] Bunsell, A.R., and B. Harris. “Hybrid Carbon and Glass Fibre Composites.” Composites 5, no. 4 (July 1974): 157–164. doi:10.1016/0010-4361(74)90107-4..

[2] Saiidi, M., F. Gordaninejad, and N. Wehbe. "Behavior of graphite/epoxy concrete composite beams." Journal of Structural Engineering 120, no. 10 (1994): 2958-2976. doi:10.1061/(ASCE)0733-9445(1994)120:10(2958).

[3] Fam, Amir Z., and Sami H. Rizkalla. “Flexural Behavior of Concrete-Filled Fiber-Reinforced Polymer Circular Tubes.” Journal of Composites for Construction 6, no. 2 (May 2002): 123–132. doi:10.1061/(asce)1090-0268(2002)6:2(123).

[4] Keller, Thomas, Erika Schaumann, and Till Vallée. “Flexural Behavior of a Hybrid FRP and Lightweight Concrete Sandwich Bridge Deck.” Composites Part A: Applied Science and Manufacturing 38, no. 3 (March 2007): 879–889. doi:10.1016/j.compositesa.2006.07.007.

[5] Correia, João R., Fernando A. Branco, and João G. Ferreira. “Flexural Behaviour of GFRP–concrete Hybrid Beams with Interconnection Slip.” Composite Structures 77, no. 1 (January 2007): 66–78. doi:10.1016/j.compstruct.2005.06.003.

[6] Correia, João Ramôa, Fernando A. Branco, and João Ferreira. “GFRP–concrete Hybrid Cross-Sections for Floors of Buildings.” Engineering Structures 31, no. 6 (June 2009): 1331–1343. doi:10.1016/j.engstruct.2008.04.021.

[7] Biddah, A. “Experimental Investigation of Pultruded Frp Section Combined With Concrete Slab.” Fibre-Reinforced Polymer Reinforcement for Concrete Structures (June 2003): 715-724. doi:10.1142/9789812704863_0067.

[8] Fam, Amir, and Trevor Skutezky. “Composite T-Beams Using Reduced-Scale Rectangular FRP Tubes and Concrete Slabs.” Journal of Composites for Construction 10, no. 2 (April 2006): 172–181. doi:10.1061/(asce)1090-0268(2006)10:2(172).

[9] Ferreira, A.J. Mendes, M.C.S. Ribeiro, and A. Torres Marques. “Analysis of Hybrid Beams Composed of GFRP Profiles and Polymer Concrete.” International Journal of Mechanics and Materials in Design 1, no. 2 (2004): 143–155. doi:10.1007/s10999-004-1493-0..

[10] Hai, Nguyen Duc, Hiroshi Mutsuyoshi, Shingo Asamoto, and Takahiro Matsui. “Structural Behavior of Hybrid FRP Composite I-Beam.” Construction and Building Materials 24, no. 6 (June 2010): 956–969. doi:10.1016/j.conbuildmat.2009.11.022.

[11] Mutsuyoshi, Hiroshi, Nguyen Duc Hai, Kensuke Shiroki, Thiru Aravinthan, and Allan Manalo. "Experimental investigation of HFRP composite beams." In Proceedings of the 10th International Symposium of the Fiber Reinforced Polymer Reinforcement for Reinforced Concrete Structures (FRPRCS-10), vol. 1, no. 275, pp. 219-243. American Concrete Institute, 2011.

[12] Gonilha, José A., João R. Correia, and Fernando A. Branco. “Structural Behaviour of a GFRP-Concrete Hybrid Footbridge Prototype: Experimental Tests and Numerical and Analytical Simulations.” Engineering Structures 60 (February 2014): 11–22. doi:10.1016/j.engstruct.2013.12.018.

[13] Nunes, Francisco, João R. Correia, and Nuno Silvestre. “Structural Behavior of Hybrid FRP Pultruded Beams: Experimental, Numerical and Analytical Studies.” Thin-Walled Structures 106 (September 2016): 201–217. doi:10.1016/j.tws.2016.05.004.

[14] Correia, Manuel Mendes. "Structural behavior of pultruded GFRP profiles experimental study and numerical modeling." Technical University of Lisbon, Av. Rovisco Pais (2012): 1001-1049.

[15] Tabkhi Wayghan, Amir Reza, Massood Mofid, Behnam Babaei Ravandi, and Seyed Morteza Zinati Yazdi. “Increasing the Contribution of GFRP Bars on the Compressive Strength of Concrete Columns with Circular Cross Section.” Civil Engineering Journal 5, no. 8 (August 25, 2019): 1850–1862. doi:10.28991/cej-2019-03091377.

[16] Zhang, Lingfeng, Weiqing Liu, Lu Wang, and Zhibin Ling. “Mechanical Behavior and Damage Monitoring of Pultruded Wood-Cored GFRP Sandwich Components.” Composite Structures 215 (May 2019): 502–520. doi:10.1016/j.compstruct.2019.02.084.

[17] Sun, Hongpeng, Mingming Jia, Sumei Zhang, and Yuyin Wang. “Study of Buckling-Restrained Braces with Concrete Infilled GFRP Tubes.” Thin-Walled Structures 136 (March 2019): 16–33. doi:10.1016/j.tws.2018.10.040.

[18] ASTM C33 / C33M, “Standard Test Method for Sieve Analysis of Fine and Coarse Aggregates”, West Conshohocken, PA. (2016), ASTM International.

[19] Designation, A. S. T. M. "C39-86." Compressive Strength of Cylindrical Concrete Specimens,"." 2002 Annual Book of ASTM Standards, American Society for Testing and Materials, Philadelphia, Pennsylvania, Section 4 (2002).

[20] ASTM A615 / A615M-16, “Standard Specification for Deformed and Plain Carbon-Steel Bars for Concrete Reinforcement.” ASTM International, West Conshohocken, PA. (2016), doi:10.1520/a0615_a0615m-16.

[21] J. R. Correia, 2004 “Glass fibre reinforced polymer (GFRP) pultruded profiles. Structural behaviour of GFRP-concrete hybrid beams.” MSc Thesis, Instituto Superior Técnico, 2004 (in Portuguese).

[22] Branco, F. A., J. Ferreira, and J. Ribeiro Correia. "The use of GRC and GFRP-concrete beams in bridge decks." In FRP composites in bridge design and civil engineering, COBRAE Conference Proceedings, Porto. (2003).

[23] Johnson, R. P. and May I. M. "Partial interaction design of composite beams." (1975).

[24] Clough, Ray W., and Joseph Penzien. "Dynamics of Structures, Computers & Structures." New York (1995).

[25] Alciatore, David G. Introduction to Mechatronics and Measurement Systems. Tata McGraw-Hill Education, (2007).

[26] Tweten, Dennis J., Zach Ballard, and Brian P. Mann. “Minimizing Error in the Logarithmic Decrement Method through Uncertainty Propagation.” Journal of Sound and Vibration 333, no. 13 (June 2014): 2804–2811. doi:10.1016/j.jsv.2014.02.024.

[27] D. D. EN., “1-1. Draft Eurocode: 4 Part 1.1, Design of Composite Steel and Concrete Structures; General Rules and Rules for Buildings, Commission of the European Communities,” Br. Stand. Inst. (1994).

[28] Srinivas, Paleti, Sambana Krishna Chaitanya Datti Rajesh Kumar, and Srinivas Paleti. Finite element analysis using ANSYS 11.0. PHI Learning Pvt. Ltd., (2010).